Nonequilibrium Solvation and the Quantum Kramers Problem: Proton Transfer in Aqueous Glycine[†]

Rakesh Karmacharya, Dimitri Antoniou, and Steven D. Schwartz*

Departments of Biophysics and Biochemistry, Albert Einstein College of Medicine, 1300 Morris Park Avenue, Bronx, New York 10461

Received: October 2, 2000; In Final Form: November 3, 2000

We study the intramolecular proton transfer in the amino acid glycine in aqueous solution. We show that this system is an example of nonequilibrium solvation, where the proton-transfer step is fast and the solvent relaxes afterward. We show how the physical picture of equilibrium vs nonequilibrium solvation arises naturally within the framework of the quantized Zwanzig Hamiltonian.

I. Introduction

In charge-transfer reactions in polar solvents it is often not sufficient to know the average response of the solvent, because the microscopic details of the solvent dynamics are crucial.[1] To give a concrete example, let us assume that the solvent molecules have a dipole moment. In one limit, assumed by the transition state theory (TST), the transferred charge moves very slowly compared to the reorientation of solvent dipoles: the effect of the solvent is to "clothe" the charge with an *equilibrium* solvation. In this picture, the reaction coordinate is solely determined by the reacting species and the appropriate potential to describe its dynamics is the mean field potential (MFP), which is a time-average of the effect of the solvent.

The other extreme limit (assumed, for example, by Marcus theory)[2] is that the transferred charge moves so quickly that the solvent dipoles are nearly frozen during the reacting event. In this limit, a *nonequilibrium* solvation description is appropriate. The potential energy surface (PES) that describes the dynamics is not some time average (like the MFP) but a specific instantaneous configuration that favors the reaction (e.g. the symmetrized potential of Marcus theory), and as a result, the reaction coordinate can be determined from the solvent.

In intermediate cases there will be a finite time of reorientation of solvent dipoles, and this lag causes a retarding effect on the transferred charge. This effect is commonly described by the generalized Langevin equation (GLE)

$$m_s\ddot{s} = -\frac{\partial \bar{V}(s)}{\partial s} + \int_0^t dt' \gamma(t-t')\dot{s} + F(t) \qquad (1)$$

where $\bar{V}(s)$ is the potential for the reaction coordinate, $F(t)$ is a fluctuating force from the solvent, and $\gamma(t)$ is the dynamic friction.

In the limit where the reorientation time of the dipoles is very small, it can be shown[3] that this equation reduces to the TST picture and the potential $\bar{V}(s)$ should be equal to the MFP. In addition, a derivation[4] of the GLE eq 1 from linear response theory suggests that deviations of GLE from the TST result can be understood as Gaussian fluctuations around the solution of GLE for a potential equal to the MFP.

In the opposite limit of nonequilibrium solvation, it is much less clear how to justify the choice of the potential $\bar{V}(s)$ in eq 1 from microscopic considerations. These questions were examined in a series of papers by van der Zwan and Hynes,[5,6] and their ideas were applied to S_N2 reactions by Hynes, Wilson, and co-workers.[7,8] A very brief summary of their findings follows.

In those studies a parabolic barrier was assumed. If $-^1/_2 m\omega_b^2 s^2$ is the bare gas-phase potential and $-^1/_2 m\omega_{eq}^2 s^2$ is the MFP barrier, it was found[7] that (in the frozen solvent limit) the barrier that is relevant for the dynamics has curvature

$$\omega^2 = \omega_{eq}^2 - \frac{1}{m_s}\gamma(t=0) \qquad (2)$$

where $\gamma(t)$ is the friction kernel from the GLE eq 1 (the value at $t = 0$ appears in eq 2 because of the frozen solvent assumption). A molecular dynamics simulation in that work showed that $\omega \approx \omega_b$; i.e., the effect of nonequilibrium solvation is to modify the MFP to almost the gas-phase potential. This result suggests a completely different picture than the equilibrium solvation limit, where (as we mentioned earlier) the dynamical effect of the solvent can be interpreted as Gaussian fluctuations around the MFP result.

More insights into the interplay between the dynamics of the solvent and the transferred charge can be provided by an alternative formulation of the GLE due to Zwanzig.[9] He proved that when the Hamiltonian

$$H = \frac{P_s^2}{2m_s} + U(s) + \sum_k \left[\frac{P_k^2}{2m_k} + \frac{1}{2}m_k\omega_k^2 \left(q_k - \frac{c_k s}{m_k\omega_k^2} \right)^2 \right] \qquad (3)$$

is integrated in the bath coordinates, the reaction coordinate s obeys the GLE eq 1 with friction

$$\gamma(t) = \sum_k \frac{c_k^2}{m_k\omega_k^2} \cos(\omega_k t) \qquad (4)$$

In eq 3, the potential $U(s)$ is defined as

$$U(s) \equiv V(s) - \sum_k \frac{c_k^2 s^2}{m_k\omega_k^2} = V(s) - \frac{1}{2}\gamma(t=0)s^2 \qquad (5)$$
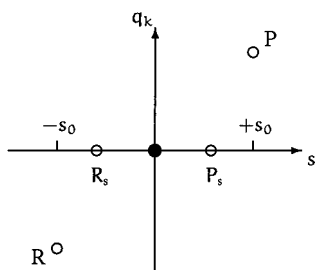
Figure 1. Locations in the (s, q_k) plane of the minima (R, P) and saddle point $(s, q_k = 0,0)$. The minima (R_s, P_s) of the potential eq 8 are also shown.

and it is equal to the MFP for the Zwanzig Hamiltonian eq 3. Any choice for the potential U leads to a GLE eq 1 with $V = U$. We must make a physically motivated choice for U. We will see in the next section why we chose U to be the MFP instead of the equally plausible (and correct) choice of the bare potential $U = V(s)$.

The hypothetical harmonic environment defined by eq 3 exerts a force equal to the force exerted by the real anharmonic environment. The Zwanzig formalism allows for a natural quantum generalization of the GLE: the Hamiltonian eq 3 is treated quantum mechanically.

At this stage, it is not at all obvious whether the Hamiltonian eq 3 can reproduce the physical pictures of equilibrium/nonequilibrium solvation described earlier in the Introduction. This will be the topic of the next section, and the conclusions will be applied on the glycine system in the last section.

II. Nonequilibrium Solvation in the Kramers Problem

We have already mentioned that an example of nonequilibrium solvation is charge transfer in the deep tunneling limit as described by Marcus theory. The physical picture suggested by Marcus theory should be obtained as a limiting case of eq 3 at the extreme quantum limit. The purpose of this section is to show how this limit is recovered. First, let us recall that the essential feature of Marcus' theory is that (in the deep tunneling limit) the reaction takes place when the environment symmetrizes the PES and that the activation energy for this to happen is equal to $E_r/4$, where E_r is the reorganization energy of the solvent (for clarity of presentation, we assume for the moment a symmetric potential $V(s)$).

The quantum version of the Hamiltonian eq 3 was first solved numerically[10] only a few years ago, for a variety of temperatures and frictions. We have developed an alternative analytical approach[11] (the exponential resummation of the evolution propagator), which has the advantage that it allows for easy calculation of high-order nonadiabatic corrections. We were able to reproduce the numerical results in the moderate quantum limit.[11] However, our method did not work well in the extreme quantum limit ($T = 100$ K) where the transmission coefficient (defined as the ratio of the exact quantum rate over the TST rate) is larger than 1000. In a later paper,[12] we were able to reproduce the exact numerical result in this extreme quantum limit, by employing a simple adiabatic approximation, with the crucial difference that we coupled the counterterm of the Hamiltonian eq 3 with the system potential, i.e., the reaction coordinate moves in the potential

$$U(s) + \sum_k \frac{c_k^2}{2m_k\omega_k^2}s^2 \qquad (6)$$

which, according to eq 5, is equal to $V(s)$. Note that if we assume that the bare potential has a parabolic form, then the potential eq 6 is equal to the van der Zwan–Hynes result eq 2. We will now explain why this potential is able to describe the quantum dynamics correctly, even in a low-level adiabatic approximation.

For clarity of presentation we will examine a simple two-dimensional case, as depicted in Figure 1 (recall that for the moment we examine the symmetric PES case), where the reaction coordinate s is coupled to a single bath oscillator q_k with frequency ω_k. The potential energy surface has the following structure:

$$\text{minima:} \quad (s, q) = \left(\mp s_0, \mp \frac{c_k s_0}{m_k \omega_k^2}\right)$$

$$\text{saddle point:} \quad (s, q) = (0, 0) \qquad (7)$$

In this 2-dimensional picture, the potential eq 6 is

$$U(s) + \frac{c_k^2 s^2}{2m_k\omega_k^2} \qquad (8)$$

Before we examine the quantum limit, we note that the minimum energy path is the trajectory $q = c_k s/m_k\omega_k^2$; i.e., it is the straight line $R-P$ that joins the minima, along which the potential is equal to the MFP $U(s) = V(s) - {}^1/_2\gamma(0)s^2$ (if we had included the notorious counterterm in the definition of the Zwanzig Hamiltonian, the MFP would be equal to the bare potential $V(s)$).

We showed in the Introduction that we expect the MFP to be the potential that reproduces the TST physical description, while the bare potential describes motion in the frozen solvent limit. In the Zwanzig Hamiltonian eq 3, our choice of $U(s)$ to be the MFP was made in order to have the MFP along the "classical" trajectory, i.e., the minimum energy path.

In any case, the above discussion shows that, in the classical limit, the Zwanzig Hamiltonian leads to a GLE with a potential equal to the MFP, which as we mentioned earlier is known[3] to correspond to the dynamics described by TST.

We now turn our attention to the extreme quantum limit. We make the following observations regarding Figure 1:

(i) The potential eq 8 is the potential along the trajectory $q_k = 0$.

(ii) The potential energy surface is symmetric along this trajectory $q_k = 0$.

These two observations show that the potential eq 8 provides the same physical description as Marcus theory, where reaction takes place along the symmetrized potential. Can the dynamics associated with the potential eq 8 reproduce the Marcus activation energy?

(iii) The reorganization energy of the 1-dimensional oscillator of our example is

$$E_r = 2s_0^2 \frac{c_k^2}{m_k\omega_k^2} \qquad (9)$$

(iv) The quantum reaction rate can be calculated using the Miller–Schwartz–Tromp formula:[13]

$$k = \frac{1}{Z_R}\int_0^{+\infty} dt\, C_f(t_c) \qquad (10)$$

where Z_R is the partition function for the reactants, $C_f(t_c)$ is the

Proton Transfer in Aqueous Glycine

J. Phys. Chem. A, Vol. 105, No. 12, 2001 **2565**

flux−flux autocorrelation function, and $t_c = t - i\beta/2$ is a complex time.

(v) We will now calculate the partition function Z_R of eq 10. We have to average this partition function Z_R over all the initial bath configurations. Remember that the considerations of this section apply to the case when the motion of the reaction coordinate is fast compared to the solvent, so we cannot take bath averages as in the equilibrium solvation case. However, the partition function Z_R is calculated with the reaction coordinate fixed, so there is no inconsistency in taking this average. The averaging over the bath initial positions leads to

$$\langle Tre^{-\beta H_S} \rangle_{bath} = Tre^{-\beta \langle H_s \rangle bath} \qquad (11)$$

which means that the partition function for the reaction coordinate is not evaluated with the bare potential $V(s)$ but with the mean field potential $V_{MFP}(s)$.

(vi) On the other hand, the correlation function C_f is evaluated with the potential eq 8, which is equal to the potential along the "sudden path" $q_k = 0$.

(vii) The previous two observations suggest that Z_R and C_f use energy eigenstates that come from diagonalizations of different potentials, which happen to have different minima. The energy difference E_a between the minima of these two potentials is implicitly built in the rate calculated by eq 10 as a factor $\exp(-\beta E_a)$.

(viii) We will now calculate this energy difference E_a. The minimum of the potential $U(s)$ (i.e. of the MFP for the Zwanzig Hamiltonian, as we explained above) is at the point R in Figure 1 and is equal to $U_{min}(s_0)$. The minimum of the "symmetrized" potential eq 8 is at $s = -\tilde{s}_0$ (the coordinate of R_s in Figure 1) and is equal to $\tilde{U}_{min}(\tilde{s}_0)$. Therefore,

$$E_a = \tilde{U}_{min}(\tilde{s}_0) - U_{min}(s_0) \qquad (12)$$

Using eq 8, this is equal to

$$E_a = \frac{c_k^2 s^2}{2m_k \omega_k^2} - [V_{min}(s_0) - V_{min}(\tilde{s}_0)] \qquad (13)$$

where $V(s)$ is the bare system potential. In a spin-boson-type Hamiltonian, it is $\tilde{s}_0 = s_0$, leading to

$$E_a = \frac{E_r}{4} \qquad (14)$$

where E_r is the reorganization energy eq 9. This result means that the factor $\exp(-\beta E_a)$, which we showed earlier that multiplies the rate eq 10, is nothing but the Marcus activation energy. The presence of the extra term $V_{min}(\tilde{s}_0) - V_{min}(s_0)$ in eq 13 is due to the fact that the minima of the $V(s)$ change in the symmetrized configuration for the type of potential we have used.

(ix) Very similar considerations are valid in the case of a biased potential. When the bare potential is not symmetric, then the path that symmetrizes the bare system potential $V(s)$ is not at $q_k = 0$ but at a point $q_k = \tilde{q}_k =$ fixed. The potential can be symmetrized by adding the term $(\Sigma_k c_k \tilde{q}_k)s = \tilde{c}s$. Though we cannot find the set $\tilde{q}_k$, all we need is a number $\tilde{c}$ such that the coupling term $\tilde{c}s$ symmetrizes $V(s)$, when the well minima are symmetrically placed with respect to the transition state at $\pm s_0$. It is $\tilde{c} = \epsilon/(2s_0)$, where ϵ is the potential bias. The "sudden" path along which the reaction takes place is then $q = \tilde{q}_k =$ fixed, and we can proceed exactly as in the symmetric case (the activation energy will turn out to have the form $(E_r - \epsilon)^2/(4E_r)$,
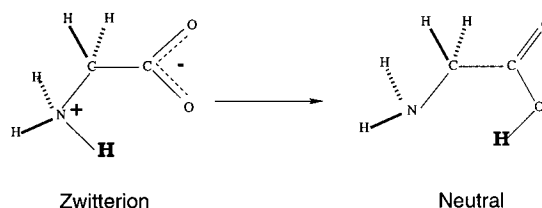

Figure 2. Intramolecular proton transfer in glycine. The transferred proton is labeled in boldface.

similar to Marcus' theory). Here we have made use of the fact that a Zwanzig Hamiltonian that has the centers of the bath oscillators shifted by $\tilde{q}_k$ leads to a GLE with the same friction $\gamma(t)$ as the original Hamiltonian eq 3.

We now summarize the results of this section: (1) In the classical limit (when the reaction coordinate follows the minimum energy path), the Zwanzig Hamiltonian leads to a GLE with a potential equal to MFP. This is an example of equilibrium solvation. (2) One example of nonequilibrium solvation, the classical motion in a frozen solvent environment as described by the van der Zwan−Hynes result eq 2, is recovered as classical motion along the potential of eq 6. (3) Another example of nonequilibrium solvation, the deep tunneling picture of Marcus theory, appears as a limiting case of the Zwanzig Hamiltonian eq 3, when we make the assumption that the flux−flux correlation function should be calculated using an adiabatic approximation and using the potential eq 6, which is the potential along the symmetrizing path of the Marcus' theory. (4) One computational scheme in this deep tunneling limit is the following: (a) Find the solvent configuration for which the bare potential is symmetrized. (b) Calculate the correlation function C_f using the potential eq 6. (c) Calculate the partition function Z_R of the reactants using the mean field potential as the potential for the reaction coordinate.

Note that we do not mix the use of gas-phase and MFP potentials. We always use the gas-phase potential in the above scheme, but the average over initial bath positions when the reaction is held fixed for the calculation of the partition function ZR leads to the appearance of the MFP.

We will apply these ideas to the glycine system in the following section.

III. Proton Transfer in Glycine

The dynamics of amino acids in aqueous solution is of paramount importance, given their pivotal roles as the building blocks for many biological macromolecules. While in the gas phase amino acids exist as nonionic neutral forms (NF), in the aqueous phase the zwitterionic forms (ZW) predominate. A prototype system to study this effect is glycine, because it is the smallest amino acid (it has only 10 atoms) and because of the availability of experimental data. Recent studies in the literature have focused on the delineation of the potential energy surface for glycine in aqueous solution and on thermodynamic investigations related to intramolecular proton transfer.[14−20]

In the gas phase the neutral form of glycine is more stable, while the zwitteronic form is more stable in the aqueous phase. In particular, the PES in the gas phase is very asymmetric, with barrier height in the ZW → NF direction equal to $V_{ZW \to NF} = 1.1$ kcal/mol, while the barrier height for the reverse direction is $V_{NF \to ZW} = 19.6$ kcal/mol.

The mean field potential for the reaction in solution is also very asymmetric but in the opposite direction; i.e., the zwitterionic form is more stable. The barrier heights are[17] $V_{ZW \to NF} = 14.4$ kcal/mol and $V_{NF \to ZW} = 7.1$ kcal/mol. It has been

suggested,[18] however, that these values depend on the level of quantum chemistry basus set used in ref 17.

The experimental values for the reaction rates and activation energy in solution are

$$k_{ZW \to NF} = 175 \text{ s}^{-1}$$

$$k_{NF \to ZW} = 4.4 \times 10^7 \text{ s}^{-1}$$

$$E_a^{ZW \to NF} = 0.4 \text{ kcal/mol} \quad (15)$$

A simple calculation shows that the TST prediction using the MFP barrier heights is too large by 3 orders of magnitude.

It has been proposed[18-20] that the reaction takes place in 2 steps: (1) The gas-phase neutral conformation is in a shallow minimum of the PES. When we place the glycine in water, there is some reorientation of amino and acid groups to a different neutral conformation, which is more favorable for proton transfer. To reach this new conformation, there is a free energy barrier 10.9 kcal/ mol. (2) From this new neutral conformation, the proton transfer is essentially barrierless.

We propose an alternative 2-step mechanism: (1) The original gas-phase neutral conformation is symmetrized by the solution. A simple calculation shows that the Marcus activation energy for this step is 1.75 kcal/mol, i.e., smaller than the energy cost for the glycine reorientation that was mentioned above. (2) The proton tunnels suddenly in the symmetrized configuration. We have checked that the symmetrized potential has height 11 kcal/ mol and transfer distance 0.7 Å; therefore, the quantum limit of the previous section applies.

The crucial point in our proposed 2-step transfer mechanism is that the proton- transfer step (Figure 2) is very fast compared to the solvation dynamics. In fact, a quantum mechanics/ molecular mechanics simulation's has verified this, showing that the proton-transfer step is very fast and takes place in a frozen solvent environment and that the solvent relaxes after the transfer step.

A. Potential Parameters. For the system under study, the total potential function V_{tot} is expressed as

$$V_{tot} = V_{RS} + V_{SS} \quad (16)$$

where V_{RS} and V_{SS} describe the solute−solvent and the solvent− solvent interactions. For our calculations, we use an analytical potential function for the glycine−water system reported by Nagaoka and co-workers.[16] This potential describes the reactive potential energy surface, as well as the interaction energy with water. The potential energy function was obtained using the empirical valence bond (EVB) method. The EVB method uses the valence bond concept with regard to ionic−covalent resonance to obtain the Hamiltonian for an isolated reactive molecule and then evaluates the Hamiltonian for the reaction in solution by adding the calculated solvation energies to the diagonal matrix of the ionic resonance forms.[21] Using this method, the potential function is written as

$$V_{RS} = \frac{1}{2}(V_{11} + V_1^{int} + V_{22} + V_2^{int}) - $$
$$\sqrt{\frac{(V_{11} + V_1^{int} + V_{22} + V_2^{int})^2}{2} + V_{12}^2} \quad (17)$$

where R refers to glycine (reactant) and S refers to water (solvent). V_{11} and V_{22} are the energies for the zwitterion (ZW) and the neutral (NF) resonance forms, respectively. V_1^{int}, and

V_2^{int}, which describe the interaction energy for the ZW−water and the NF−water interactions, respectively, are of the form described by Clementi and co-workers[22-24]

$$V_k^{int} = \sum_{i \in solute} \sum_n^{(water)} \sum_{j \in nth} \left[\frac{A_{ij}^{(k)}}{R_{ij}^{12}} - \frac{B_{ij}^{(k)}}{R_{ij}^6} + \frac{C_{ij}^{(k)} q_i q_j}{R_{ij}} \right] \quad (18)$$

where R_{ij} is the distance between the atom i on glycine and the atom j of the nth water. The square of the exchange matrix element V_{12}^2 is described using the form employed by Chang and Miller:[25,26]

$$V_{12}^2 = A_{exch} \exp\left(B_{exch}^T \Delta q - \frac{1}{2} \Delta q^T C_{exch} \Delta q \right) \quad (19)$$

where Δq is the deviation from the reference geometry (transition state in our case.)

The potential eqs 16−19 were chosen in ref 17 so that they reproduce the set of energies and forces calculated at the HF/ 6-31+G* level. A relatively small basis set was employed because the calculation of electronic energies and forces were required at many points and because it could reproduce some results that had been derived with the use of a larger basis set. More recent explorations and advances on this topic can be found in refs 18−20.

For the solvent−solvent interaction, we use the TIP4P model.[27,28] The TIP4P model is a 4-site model, where the negative charge is moved off the oxygen and toward the hydrogens, at a point M on the bisector of the HOH angle. In this model, there is intermolecular Coulombic interaction between the hydrogen atoms and the M site and Lennard-Jones interaction between the oxygen atoms[27,28]

$$V_{ij}^{TIP4P} = \sum_{i \in mth} \sum_{j \in nth} \left[\frac{q_i q_j e^2}{R_{ij}} + \frac{A_{oo}}{R_{oo}^{12}} - \frac{B_{oo}}{R_{oo}^6} \right] \quad (20)$$

with $A_{oo} = 600\ 000 \text{ Å}^{12} \text{ kcal/mol}$ and $B_{oo} = 610 \text{ Å}^6/\text{mol}$. The charge on the hydrogen atoms is $q_H = 0.52$, and the charge at the ghost site is $q_M = 1.04$. In the TIP4P model the HOH angle is 104.52°, the O−H distance is 0.9572 Å, and the distance from the M site to the O site is 0.15 Å. TIP4P yields the correct density for liquid water and has been shown to reproduce experimental and structural data at 25 °C and 1 atm.[29]

B. Molecular Dynamics. The purpose of the MD simulations here is to calculate the dynamic friction $\gamma(t)$ exerted on the transferred proton in glycine, which is then used as an input for the Zwanzig Hamiltonian in the form of its cosine Fourier transform, which is the spectral density $J(\omega)$. Using the potential parameters described above, we performed molecular dynamics simulations placing one glycine molecule and 255 water molecules in a cubic box with side 19.75 Å. The coordinates of glycine were fixed using the bond distance and angle parameters for the gas-phase transition state,[17] for the reasons that were explained in the previous section. The box length and number of water molecules were chosen to correspond to 0.997 g/cm³, the mass density of glycine−water solution at room temperature.

The equations of motion were integrated using the modified RATTLE algorithm,[30] which incorporates the constraint method that was originally developed for the SHAKE algorithm.[31] The long-range Coulombic forces for the water−water and glycine− water interactions were spherically truncated to zero at $r_c = 9.84$ Å using a smoothing function.[32]

Proton Transfer in Aqueous Glycine

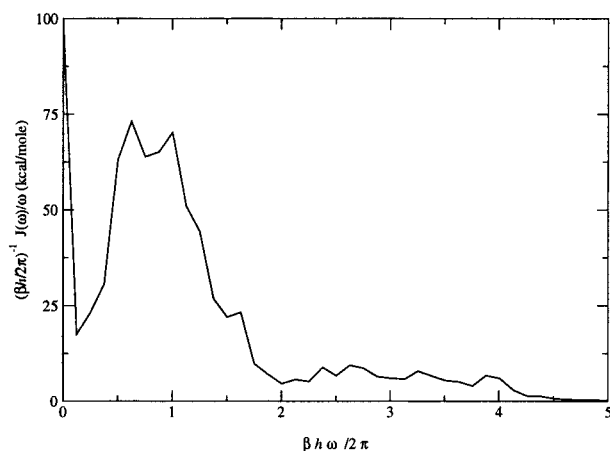*J. Phys. Chem. A, Vol. 105, No. 12, 2001* **2567**

Figure 3. Quantity $J(\omega)/\omega$ for the transferred proton in aqueous solution calculated from our molecular dynamics simulation. The frequency is in reduced units of $\beta\hbar$, in which a unit of 1 corresponds to a frequency $\omega = 200$ cm^{-1}.

The molecular dynamics simulations were carried out with a time step $\Delta t = 0.1$ fs. After equilibrating for 10 ps, the MD trajectories were run for 10 ps. During the MD simulation, the transferring proton was held fixed in the gas transition state configuration.[17] The force on the proton was recorded for each time step and used to calculate the dynamical friction $\gamma(t)$. By taking the inverse Fourier cosine transform of $\gamma(t)$, we calculated the spectral density $J(\omega)$.

Figure 3 shows a plot of the spectral density $J(\omega)/\omega$ as a function of the frequency ω.

IV. Results and Discussion

Once we obtain the spectral density $J(\omega)$, we can proceed with the calculation of the quantum rate using the Miller−Schwartz−Tromp formula eq 10. The flux−flux correlation function that appears there is calculated from

$$C_f = \frac{1}{4m^2} \int dq \int dq' \left[\frac{\partial^2}{\partial s \partial s'} \left| \langle s'q'|e^{-iHt_c}|sq \rangle \right|^2 - 4 \left| \frac{\partial}{\partial s'} \langle s'q'|e^{-iHt_c}|sq \rangle \right|^2 \right]_{s=s'=0} \quad (21)$$

where $H = H_s + H_q + f$ is the total Hamiltonian. Details of the evaluation of eq 21 can be found in our earlier publications.[11,12]

For the quantum calculation we followed the scheme outlined in section II, which requires the bare system potential. To calculate the partition function Z_R appearing in eq 10, we need the MFP and not the bare potential; as we explained in the previous section, we used the MFP calculated in an earlier simulation[17] and for the reactant and product frequencies we used the experimental value[15] $\omega_{NH} = 3058$ cm^{-1}. We obtained the following results:

$$k_{ZW \to NF} = 750 \text{ s}^{-1}$$

$$k_{NF \to ZW} = 6.6 \times 10^7 \text{ s}^{-1}$$

$$E_a^{ZW \to NF} = 1.2 \text{ kcal/mol} \quad (22)$$

They are in good agreement with the experimental results eq 15.

In the last 5 years, there has been substantial progress in developing methods for the numerical solution of the quantum Hamiltonian eq 3 for proton transfer, where there is no small perturbation parameter. In this paper we examined some of the subtleties that remain to be resolved before these numerical methods are applied to realistic systems.

In classical charge transfer, the equilibrium solvation picture assumed by TST is well understood. The nonequilibrium solvation picture is far less clear, but a series of papers by Hynes and co-workers lead to the result eq 2. In section II we used a simple two-dimensional PES and showed how these two solvation pictures are recovered in different limits of the classical Zwanzig Hamiltonian. We then examined the quantum Zwanzig Hamiltonian in the deep tunneling limit. We showed that a simple adiabatic approximation for the evolution operator gives good numerical results when the flux-flux correlation function is evaluated using the potential eq 6, because this is the potential along the PES-symmetrizing sudden tunneling path of the Marcus theory. In addition, the potential along this path is the same as the potential eq 2 used in Hynes' classical nonequilibrium solvation theory.

References and Notes

(1) Hynes, J. T. *Annu. Rev. Phys. Chem.* **1985**, *36*, 573.
(2) Benderskii, V.; Makarov, D.; Wight, C. *Adv. Chem. Phys.* **1994**, *88*, 1.
(3) Chandler, *D. J. Chem. Phys.* **1978**, *68*, 2959.
(4) Chandler, D. *Statistical Mechanics*; Oxford University Press: Oxford, U.K., 1987.
(5) van der Zwan, G.; Hynes, J. T. *J. Chem. Phys.* **1982**, *76*, 2993.
(6) van der Zwan, G.; Hynes, J. T. *J. Chem. Phys.* **1983**, *78*, 4174.
(7) Bergsma, J. P.; Gertner, B. J.; Wilson, K. R.; Hynes, J. T. *J. Chem. Phys.* **1987**, *86*, 1356.
(8) Gertner, B. J.; Bergsma, J. P.; Wilson, K. R.; Kee, S.; Hynes, J. T. *J. Chem. Phys.* **1987**, *86*, 1377.
(9) Zwanzig, R. *J. Stat. Phys.* **1973**, *9*, 215.
(10) Topaler, M.; Makri, N. *J. Chem. Phys.* **1994**, *101*, 7500.
(11) Schwartz, S. D. *J. Chem. Phys.* **1996**, *105*, 6871.
(12) Schwartz, S. D. *J. Chem. Phys.* **1997**, *107*, 2424.
(13) Miller, W. H.; Schwartz, S. D.; Tromp, J. W. *J. Chem. Phys.* **1983**, *79*, 4889.
(14) Jensen, J. H.; Gordon, M. S. *J. Am. Chem. Soc.* **1995**, *117*, 8159.
(15) Tortonda, F. R.; Pascual-Ahuir, J. L.; Silla, E.; Tunon, I.; Ramirez, F. J. *J. Chem. Phys.* **1998**, *109*, 592.
(16) Okuyama-Yoshida, N.; Nagaoka, M.; Yamabe, T. *J. Phys. Chem. A* **1998**, *102*, 285.
(17) Nagaoka, M.; Okuyama-Yoshida, N.; Yamabe, T. *J. Phys. Chem. A* **1998**, *102*, 8202.
(18) Tunon, I.; Silla, E.; Millot, C.; Martins-Costa, T.; Ruiz-Lopez, M. F. *J. Phys. Chem. A* **1998**, *102*, 8673.
(19) Tunon, I.; Silla, E.; Ruiz-Lopez, M. F. *Chem. Phys. Lett.* **2000**, *321*, 433.
(20) Tortonda, F. R.; Silla, E.; Tunon, I.; Rinaldi, D.; Ruiz-Lopez, M. E *Theor. Chem. Acc.* **2000**, *104*, 89.
(21) Warshel, A. *Computer Modeling of Chemical Reactions in Enzymes and Solutions*; John Wiley & Sons: New York, 1991.
(22) Romano, S.; Clementi, E. *Int. J. Quantum Chem.* **1978**, *14*, 839.
(23) Clementi, E.; Cavallone, F.; Scordamaglia, R. *J. Am. Chem. Soc.* **1977**, *99*, 5531.
(24) Carozzo, L.; Corongiu, G.; Petrongolo, C.; Clementi, E. *J. Phys. Chem.* **1978**, *68*, 787.
(25) Chang, Y.-T.; Miller, W. H. *J. Phys. Chem.* **1990**, *94*, 5884.
(26) Miller, W. H. *J. Phys. Chem.* **1991**, *95*, 9428.
(27) Jorgensen, W. L.; Chandrasekhar, J.; Madura, J.; Impey, R.; Klein, M. *J. Chem. Phys.* **1983**, *79*, 926.
(28) Jorgensen, W. L.; Madura, J. *Mol. Phys.* **1985**, *56*, 1381.
(29) Neumann, M. *J. Chem. Phys.* **1986**, *85*, 1567.
(30) Hurley, M.; Hammes-Schiffer, S. *J. Phys. Chem. A* **1997**, *101*, 3977−3989.
(31) Ciccotti, G.; Ferrario, M.; Ryckaert, J. *Mol. Phys.* **1982**, *47*, 1253.
(32) Steinhauser, O. *Mol. Phys.* **1982**, *45*, 335.